




Spin current density functional theory of Weyl semimetalsFilippo Bodo ¹, Jacques K. Desmarais ^{1,2,*} and Alessandro Erba ^{1,†}¹*Dipartimento di Chimica, Università di Torino, via Giuria 5, 10125 Torino, Italy*²*Equipe de Chimie Physique, IPREM UMR5254, Université de Pau et des Pays de l'Adour, Pau, France*

(Received 18 December 2021; revised 15 February 2022; accepted 22 February 2022; published 8 March 2022)

Weyl fermions are massless solutions of the Dirac equation described by two-component ($2c$) complex spinors. Such elusive objects emerge as quasiparticles in so-called Weyl semi-metals (WSM). We discuss the generalization of the standard one-component density functional theory (DFT) to a $2c$ approach (the spin-current density functional theory, SCDFT), and its application to the practical quantum-mechanical description of WSMS through a self-consistent treatment of the spin-orbit coupling (SOC) and nonlocal Fock exchange. For hybrid exchange-correlation functionals in the local density approximation or generalized gradient approximation of the SCDFT, we use Levy's constrained search formalism to map specific blocks of the SCDFT potential to specific blocks of the one-electron density matrix, which allows for a straightforward comparison of SCDFT with DFT. We show how a three-dimensional doubly degenerate bulk Dirac node is present in the TaAs WSM in the absence of SOC, lying on the $k_x = 0$ mirror plane, which is split into two singly degenerate Weyl nodes off the mirror plane by the SOC. This breaking of the degeneracy and the corresponding splitting of the two Weyl nodes with opposite chirality offers a measurable way to assess different theories. We show how an SCDFT formulation is essential to a correct quantitative description of the electronic features of WSMS.

DOI: [10.1103/PhysRevB.105.125108](https://doi.org/10.1103/PhysRevB.105.125108)**I. INTRODUCTION**

Weyl fermions are chiral massless spin-1/2 particles named after Hermann Weyl who theorized them as possible solutions of the two-component Weyl equation back in 1929 [1–3]. The actual existence of such particles remained elusive until about the early 2010s when it was theoretically understood that they could emerge as quasiparticles in certain crystals with peculiar features in the electronic band structure: the so-called Weyl semimetals (WSMs) [4–7]. A WSM is characterized by singly degenerate electronic bands, which cross at specific points (referred to as Weyl nodes) in the Brillouin zone with a linear dispersion along all three directions in momentum space. Pictorially, Weyl nodes can be interpreted as three-dimensional (3D) analogs of the two-dimensional (2D) Dirac cones of graphene [8]. At variance with topological insulators where only surface states are relevant to their peculiar electronic properties [9,10], WSMS also exhibit bulk states responsible for a variety of exotic phenomena such as the anomalous Hall effect, nonlocal transport, negative magnetoresistance, unusual optical conductivity, and local nonconservation of the ordinary current [11–14]. Many crystals have since been theoretically suggested as possible WSM candidates, with a broken space inversion symmetry [15–20] or time-reversal symmetry [21,22]. However, none of them proved stable and simple enough to be successfully synthesized.

In 2015, an ideal, stoichiometric, time reversal symmetry-preserving WSM candidate was found through a computational screening over hundreds of possible non-centrosymmetric crystals: tantalum arsenide, TaAs, in its tetragonal $I4_1md$ space group. Standard density functional theory (DFT) was used to characterize its 3D electronic band structure, as well as its electronic surface states [23]. The inclusion of spin-orbit coupling (SOC) into the DFT treatment proved crucial to be able to find, locate, and characterize the Weyl nodes in its electronic structure [23,24]. A total of 24 Weyl nodes were found in the bulk Brillouin zone of the crystal that could be grouped into two independent families: 8 nodes (denoted as W1) lying on the $k_z = 1$ plane (in units of $2\pi/c$), and 16 nodes (denoted as W2) lying off this plane. In turn, each Weyl node belongs to a pair of nodes with opposite chirality. Shortly after, in 2015, building on these theoretical predictions, came the experimental confirmation of the WSM character of TaAs through a soft x-ray angle-resolved photoemission spectroscopy (XS-ARPES) investigation of its bulk and surface electronic structure: the 3D linearly dispersed Weyl cones and the corresponding Fermi arc surface states were first revealed [25] and then confirmed [26–28]. Quantum-mechanical simulations based on the DFT not only initially predicted the WSM nature of TaAs [23], but were systematically used since to characterize its many peculiar electronic, optical, and mechanical properties [29–37]. DFT simulations also proved key to the prediction of a high-pressure hexagonal phase of TaAs belonging to the $P6m2$ space group [38]. The new phase emerges above about 14 GPa of pressure, can be stabilized at ambient conditions, and, remarkably, is in turn a WSM with 12 Weyl nodes of just one type [39].

*jacqueskontak.desmarais@unito.it

†alessandro.erba@unito.it

II. FORMAL ASPECTS

We briefly recalled above the crucial role that DFT simulations have played and likely will keep playing in the prediction and characterization of WSMs, representing the method-of-choice for affordable solid-state quantum-mechanical simulations. However, Weyl fermions are intrinsically two-component ($2c$) complex spinors [1] while standard DFT approaches are devised on a one-component ($1c$) real spinor representation of the wave function [40], which makes them unsuitable to a quantitative description of many electronic properties of WSMs, as illustrated below. The generalization of the standard $1c$ DFT to a more general description where the wave function is expressed in the basis of $2c$ Pauli spinors, known as spin current density functional theory (SCDFT), was first developed for a treatment of arbitrarily oriented magnetic fields [41] and later extended to the treatment of SOC [42]. To fully capture the complex $2c$ nature of the wave function, exchange-correlation (xc) functionals of the SCDFT must depend on an extended set of density variables [41–47]:

$$\text{DFT: } F_{\text{xc}}[n], \quad (1)$$

$$\text{collinear SDFT: } F_{\text{xc}}[n, m_z], \quad (2)$$

$$\text{noncollinear SDFT: } F_{\text{xc}}[n, m_x, m_y, m_z], \quad (3)$$

$$\text{SCDFT: } F_{\text{xc}}[n, m_x, m_y, m_z, \mathbf{j}, \mathbf{J}^x, \mathbf{J}^y, \mathbf{J}^z], \quad (4)$$

where n is the particle-number density; m_x, m_y , and m_z are the Cartesian components of the magnetization vector \mathbf{m} ; \mathbf{j} is the particle current; and $\mathbf{J}^x, \mathbf{J}^y, \mathbf{J}^z$ the three spin-current vector densities. For the different DFT schemes outlined in Eqs. (1) to (4), xc potentials \hat{v}_{xc} are defined through appropriate functional derivatives of the xc energy, E_{xc} . For instance,

$$\text{DFT: } \hat{v}_{\text{xc}} = \frac{\delta E_{\text{xc}}}{\delta n}, \quad (5)$$

$$\text{collinear SDFT: } \hat{v}_{\text{xc}} = \frac{\delta E_{\text{xc}}}{\delta n} + \sigma^z \frac{\delta E_{\text{xc}}}{\delta m_z}, \quad (6)$$

$$\text{noncollinear SDFT: } \hat{v}_{\text{xc}} = \frac{\delta E_{\text{xc}}}{\delta n} + \sum_c^{x,y,z} \sigma^c \frac{\delta E_{\text{xc}}}{\delta m_c}, \quad (7)$$

where σ^x, σ^y , and σ^z are Pauli spin matrices. We refer to Eqs. (7) to (9) of Ref. [48] for analogous expressions for the case of SCDFT. For time reversal symmetry (TRS) preserving crystals, such as TaAs, the magnetization \mathbf{m} and particle-current \mathbf{j} are vanishing, hence Eq. (4) reduces to [41,42,47]

$$\text{SCDFT (TRS): } F_{\text{xc}}[n, \mathbf{J}^x, \mathbf{J}^y, \mathbf{J}^z]. \quad (8)$$

Thus, in analogy with scalar-relativistic theories, \mathbf{j} and \mathbf{m} in SCDFT are nonvanishing in open-shell systems only, and characterize field-free, as well as Abelian field-response properties of the system [41,49–51]. On the other hand, $\mathbf{J}^x, \mathbf{J}^y, \mathbf{J}^z$ are nonvanishing even in closed-shell systems and may be interpreted as responses to an effective, non-Abelian field produced by the SOC effect [49,52].

The explicit parametrization of xc functionals of the type (4) or (8) is a formidable task and has never been attempted, which explains the very limited application of the SCDFT in condensed matter physics to date [53]. Recently, a formal analysis of the nonlocal Fock exchange operator \hat{X} in a $2c$ complex spinor basis has allowed us to identify specific spin-blocks associated to specific density variables [54]. The matrix representation \mathbf{X} of \hat{X} in a given single-particle orbital basis in spin space is

$$\mathbf{X} = \text{Re} \begin{pmatrix} \mathbf{X}^{\uparrow\uparrow} & \mathbf{X}^{\uparrow\downarrow} \\ \mathbf{X}^{\downarrow\uparrow} & \mathbf{X}^{\downarrow\downarrow} \end{pmatrix} + \text{Im} \begin{pmatrix} \mathbf{X}^{\uparrow\uparrow} & \mathbf{X}^{\uparrow\downarrow} \\ \mathbf{X}^{\downarrow\uparrow} & \mathbf{X}^{\downarrow\downarrow} \end{pmatrix}. \quad (9)$$

For instance, in a basis of pure real local orbitals ($\phi_\mu, \phi_\nu, \phi_\rho, \phi_\omega, \dots$), the matrix elements of \mathbf{X} are written [47]

$$X_{\mu\nu}^{\sigma\sigma'} = \sum_{\rho\omega} P_{\rho\omega}^{\sigma\sigma'} (\mu\rho|\omega\nu), \quad (10)$$

where σ and $\sigma' = \uparrow, \downarrow$ are spin indices, $(\dots|\dots)$ is a two-electron integral written in Mulliken notation, and $P_{\mu\nu}^{\sigma\sigma'}$ are elements of the one-electron density matrix \mathbf{P} . Equation (10) provides a one-to-one mapping of the spin-blocks of the one-electron density matrix to those of the Fock exchange matrix. The spin-blocks of \mathbf{P} (and hence of \mathbf{X}) are, in turn, linked to individual density variables. Specifically [47,54],

$$\begin{aligned} \text{Re}\mathbf{X}^{\uparrow\uparrow} + \text{Re}\mathbf{X}^{\downarrow\downarrow} &\longleftrightarrow n, \\ \text{Re}\mathbf{X}^{\downarrow\uparrow} + \text{Re}\mathbf{X}^{\uparrow\downarrow} &\longleftrightarrow m_x, \\ \text{Im}\mathbf{X}^{\downarrow\uparrow} - \text{Im}\mathbf{X}^{\uparrow\downarrow} &\longleftrightarrow m_y, \\ \text{Re}\mathbf{X}^{\uparrow\uparrow} - \text{Re}\mathbf{X}^{\downarrow\downarrow} &\longleftrightarrow m_z, \\ \text{Im}\mathbf{X}^{\uparrow\uparrow} + \text{Im}\mathbf{X}^{\downarrow\downarrow} &\longleftrightarrow \mathbf{j}, \\ \text{Im}\mathbf{X}^{\downarrow\uparrow} + \text{Im}\mathbf{X}^{\uparrow\downarrow} &\longleftrightarrow \mathbf{J}^x, \\ \text{Re}\mathbf{X}^{\downarrow\uparrow} - \text{Re}\mathbf{X}^{\uparrow\downarrow} &\longleftrightarrow \mathbf{J}^y, \\ \text{Im}\mathbf{X}^{\uparrow\uparrow} - \text{Im}\mathbf{X}^{\downarrow\downarrow} &\longleftrightarrow \mathbf{J}^z. \end{aligned} \quad (11)$$

Stemming from this analysis and from that of the short range behavior of the exchange hole [49] we propose a formally sound, and yet practical, version of the SCDFT, which consists in the inclusion of a fraction α of Fock exchange into otherwise standard xc potentials \hat{v}_{xc} of the SDFT or DFT [48] as follows:

$$\text{SCDFT: } \hat{v}_{\text{xc}}[n, \mathbf{m}, \mathbf{j}, \mathbf{J}^x, \mathbf{J}^y, \mathbf{J}^z] = \hat{v}_c[n, \mathbf{m}] + (1 - \alpha) \times \hat{v}_x[n, \mathbf{m}] + \alpha \times \hat{X}[n, \mathbf{m}, \mathbf{j}, \mathbf{J}^x, \mathbf{J}^y, \mathbf{J}^z], \quad (12a)$$

$$\text{SDFT (TRS): } \hat{v}_{\text{xc}}[n, \mathbf{J}^x, \mathbf{J}^y, \mathbf{J}^z] = \hat{v}_c[n] + (1 - \alpha) \times \hat{v}_x[n] + \alpha \times \hat{X}[n, \mathbf{J}^x, \mathbf{J}^y, \mathbf{J}^z], \quad (12b)$$

where α is a single tunable parameter in the theory, as in the well-known global hybrid standard xc functionals [55,56]. In Eq. (12), \hat{v}_c and \hat{v}_x are the correlation and exchange potential

operators in either a local density approximation (LDA) or generalized gradient approximation (GGA) treatment [48]. To assess the effect of the current densities (such as \mathbf{j} and

$\mathbf{J}^x, \mathbf{J}^y, \mathbf{J}^z$) on the electronic structure, we devise a strategy to selectively “turn-off” their contributions in the exchange operator \hat{X} , as worked out in the electronic supporting infor-

mation (ESI) [57]. This procedure leads to an operator \hat{X}' that does not depend on the current densities. Thus, in terms of \hat{X}' , Eqs. (12a) and (12b) reduce to

$$\text{SCDFT} \rightarrow \text{SDFT: } \hat{v}_{xc}[n, \mathbf{m}] = \hat{v}_c[n, \mathbf{m}] + (1 - \alpha) \times \hat{v}_x[n, \mathbf{m}] + \alpha \times \hat{X}'[n, \mathbf{m}], \quad (13a)$$

$$\text{SCDFT (TRS)} \rightarrow \text{DFT: } \hat{v}_{xc}[n] = \hat{v}_c[n] + (1 - \alpha) \times \hat{v}_x[n] + \alpha \times \hat{X}'[n]. \quad (13b)$$

Hence, the comparison of predictions from Eqs. (12b) and (13b) allows for a clearer understanding of the role played by the spin current densities in the two-electron potential.

III. COMPUTATIONAL DETAILS

All calculations are performed with a developmental version of the CRYSTAL17 package [58,59], which has recently been generalized to the self-consistent treatment of SOC [46,47,60], and where we implemented the approach described in Sec. II. We used the ECP60MDF and ECP28MDF effective-core potentials of Dolg and coworkers, for Ta and As, respectively [61,62]. These were derived from multiconfigurational four-component Dirac-Coulomb Breit calculations and were used with valence basis sets derived from the associated quadruple-zeta ones [61,62]. For Ta, we removed all polarization functions with exponents below 0.1 a.u., resulting in a final $(9s8p5d)/[5s5p3d]$ valence basis set for the 13 valence electrons in the solid. Also for As, polarization functions with exponents below 0.1 a.u. were removed, resulting in a final $(5s4p)/[3s2p]$ contraction for the five valence electrons in the solid. Reciprocal space is sampled on a regular $30 \times 30 \times 30$ Monkhorst-Pack net within the reciprocal primitive cell, which corresponds to 27 000 independent \mathbf{k} points when symmetry is not exploited (for single-point calculations upon inclusion of SOC) or to 1992 independent \mathbf{k} points when symmetry is exploited (for geometry optimizations without SOC). Convergence is achieved when the difference in energy between two successive cycles does not exceed 1×10^{-8} a.u. Calculations are performed using the SVWN5 exchange-correlation (xc) functional of the LDA. Truncation of the Coulomb and exchange infinite lattice series is controlled by five parameters, which are here set to 8, 8, 8, 8, 20 (see TOLINTEG keyword in the Manual).

IV. RESULTS AND DISCUSSION

In this paper, we report the first application of the SCDFT to a WSM, TaAs, where the simultaneous self-consistent treatment of SOC and Fock exchange proves key to a correct description of its peculiar bulk electronic features (notably, of its Weyl nodes). Predictions from the SCDFT are compared to those from standard DFT and assessed on available ARPES experimental data. We show how a 3D bulk Dirac node is present in the absence of SOC, lying on the $k_x = 0$ mirror plane, which is split into two W1 Weyl nodes off the mirror plane by the SOC. This breaking of the degeneracy and the corresponding splitting of the two W1 nodes with opposite chirality offers a measurable way to assess different theories. We discuss how an SCDFT formulation is essential

to a correct quantitative description of the electronic features of WSMs.

Calculations are performed on fully relaxed TaAs structures under the only constraints imposed by the $I4_1md$ tetragonal space group. Figure 1 (left) shows the atomic structure of the TaAs tetragonal lattice. We start by discussing the orbital relaxation of the spin current densities \mathbf{J}^x , \mathbf{J}^y , and \mathbf{J}^z during the self-consistent-field (SCF) process with SOC included for the different theories introduced in Sec. II. Figure 1 (right) reports the differences of spin current densities between the final electronic solution and the initial one (where the initial one corresponds to the so-called “second variational” density obtained after the first diagonalization of the full Hamiltonian matrix starting from the scalar relativistic solution) of the SCF process: $\Delta \mathbf{J}^c = \mathbf{J}_{\text{final}}^c - \mathbf{J}_{\text{initial}}^c$, with $c = x, y, z$. The various panels show color maps of the spatial distribution of such differences in a plane defined by the \mathbf{a} and \mathbf{c} lattice vectors of TaAs, which passes through Ta and As atoms shown in the upper left panel. The color identifies the absolute value of the reported quantity while the length and direction of the superimposed black arrows represent the magnitude and direction of their in-plane Cartesian components. It is clearly seen that both a nonhybrid standard DFT (with $\alpha = 0$) and a

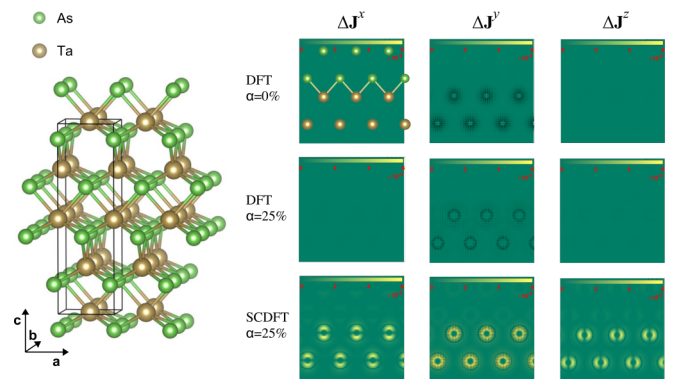


FIG. 1. (Left) Atomic structure of the $I4_1md$ tetragonal lattice of TaAs. (Right) Effect of orbital-relaxation on spin-current densities during the self-consistent-field process. The reported quantities are differences between the final electronic solution and the initial one: $\Delta \mathbf{J}^c = \mathbf{J}_{\text{final}}^c - \mathbf{J}_{\text{initial}}^c$, with $c = x, y, z$. A plane defined by the \mathbf{a} and \mathbf{c} lattice vectors of the TaAs WSM was selected, which passes through Ta and As atoms shown in the upper left panel. The various panels show color maps of the spatial distribution of $\Delta \mathbf{J}^x$, $\Delta \mathbf{J}^y$, and $\Delta \mathbf{J}^z$ in such a plane. The color identifies the absolute value of the reported quantity while the length and direction of the superimposed black arrows represent the magnitude and direction of their in-plane Cartesian components (no arrows are visible for $\Delta \mathbf{J}^x$ and $\Delta \mathbf{J}^z$ as they happen to be orthogonal to the selected plane).

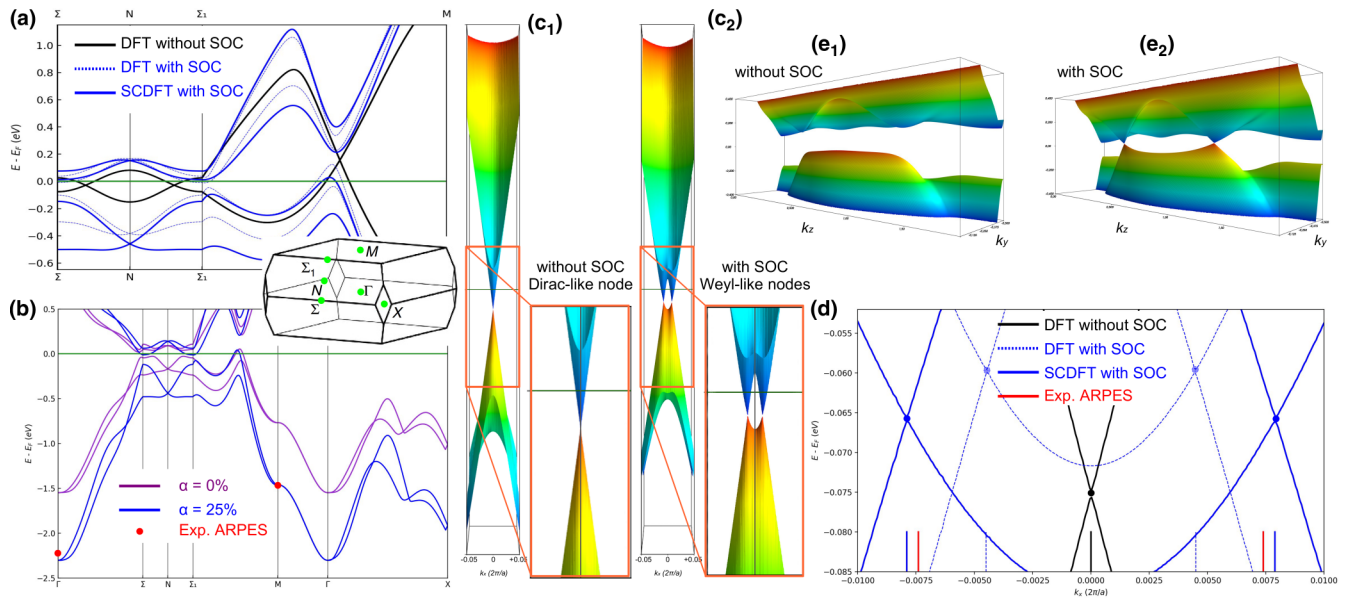


FIG. 2. Bulk electronic structure of TaAs from SCDFT: (a) Electronic band structure along the $\Sigma-N-\Sigma_1-M$ path within the conventional Brillouin zone [shown between panels (a) and (b)] without SOC and with SOC both in a DFT and SCDFT formulation. (b) Electronic band structure along the $\Gamma-\Sigma-N-\Sigma_1-M-\Gamma-X$ path as obtained without inclusion of Fock exchange ($\alpha = 0$) and with inclusion of 25% of Fock exchange ($\alpha = 0.25$). Available experimental data from ARPES measurements are also reported [26]. (c₁, c₂) 3D representation of the band structure in the region of the W1 Weyl nodes, without and with inclusion of SOC, respectively. (d) Location of W1 Weyl nodes along the k_x coordinate without SOC and with SOC both in a DFT and SCDFT formulation. The experimental location derived from ARPES measurements is marked by a vertical red line [26]. (e₁, e₂) 3D representation of the band structure in the region of the W2 Weyl nodes, without and with inclusion of SOC, respectively.

hybrid DFT (with $\alpha \neq 0$) of the type (13b) are not capable of accounting for the relaxation of such density variables. Instead, a SCDFT approach of the type (12b) allows for the effective relaxation of the spin-current densities throughout the SCF process as a result of the coupling with the spin-orbit interaction.

As introduced in Eq. (12b), the only tunable parameter of our theory is the fraction α of Fock exchange. Therefore, we started by determining the optimal value for such parameter by exploring the range 0–50% at steps of 5% through comparison of computed electronic band structures to available experimental data from ARPES measurements [26]. An optimal value of $\alpha = 25\%$ was found, as shown in Fig. 2(b) where the electronic structure of TaAs (top of valence and bottom of conduction bands only) is shown along the $\Gamma-\Sigma-N-\Sigma_1-M-\Gamma-X$ path in the conventional Brillouin zone, with SOC being taken into account. The results obtained with other values of α are given in the ESI. It is worth pointing out that an optimal value of $\alpha = 25\%$ is very consistent with typical values used in standard hybrid DFT functionals [56,63]. To highlight the effect of SOC on the electronic structure of TaAs, and to show how critically it depends on the use of the SCDFT of Eq. (12b) versus the DFT of Eq. (13b), in Fig. 2(a) we analyze the electronic band structure in the vicinity of the Fermi level E_F of the system (green line) along the $\Sigma-N-\Sigma_1-M$ path, as obtained with $\alpha = 25\%$. In the absence of SOC (black lines), the solution is metallic with both the top of valence and bottom of conduction bands crossing E_F and each other and being doubly degenerate. When SOC is taken into account (blue lines), the degeneracy is broken so that both the top of the valence and the bottom of the conduction bands

are split. Moreover, the valence and conduction bands are separated and the electronic structure becomes fully gapped along the high-symmetry path. The splitting of the bands induced by SOC is drastically enhanced by the use of the SCDFT (solid lines) with respect to the DFT (dotted lines), particularly so for the top of the valence band where the SCDFT splitting is twice as large the DFT one.

Crucially, the spin-orbit interaction induces the formation of two families of Weyl nodes, W1 and W2, off high-symmetry planes in the Brillouin zone. We performed a 3D scan of the Brillouin zone and located the Weyl nodes. Figure 2(e) shows a 3D representation of the electronic band structure close to the Fermi level in the region of the W2 nodes (i.e., in the k_y-k_z plane at $k_x = 0.0127$, in units of $2\pi/a$), without and with SOC. Contrarily to what was suggested by previous DFT calculations [23], the electronic structure of TaAs appears fully gapped in the region of W2 before inclusion of SOC, which then induces the formation of the W2 nodes, as expected. We believe that the most relevant bulk electronic feature of the TaAs WSM is represented by the W1 family of Weyl nodes. Indeed, present SCDFT calculations show for the first time that a 3D Dirac-like doubly degenerate node exists in the absence of SOC, which lies on a mirror plane at $k_x = 0$. The spin-orbit interaction again breaks the degeneracy and induces the splitting of the Dirac-like node into two singly degenerate Weyl nodes of opposite chirality off the mirror plane along the k_x direction. This is shown in Fig. 2(c) where a 3D representation of the electronic band structure is reported close to the Fermi level in the region of the W1 nodes (i.e., in the k_x-k_y plane at $k_z = 1$, in units of $2\pi/c$), without and with SOC. The splitting of the Dirac node into

the two Weyl nodes off the $k_x = 0$ mirror plane was measured experimentally [26] and offers a way to quantitatively assess different theories. Figure 2(d) shows one-dimensional (1D) profiles of the band structure along the k_x axis in the region of the W1 Weyl nodes. The Dirac-like doubly degenerate node is seen at $k_x = 0$ (black line). The splitting into two Weyl nodes described by the SCDFT is about twice as large as that obtained by the DFT (solid versus dotted blue lines) and is remarkably close to the experimentally observed splitting by ARPES measurements (the position of the Weyl nodes being marked by vertical lines at the bottom of the panel) [26].

In summary, we illustrated the spin-current density functional theory of Weyl nodes in Weyl semi-metals and we

applied it to the description of the electronic features of TaAs. The specific aspects of the theory which make it suitable to the quantitative description of WSMs are discussed and the overall effectiveness of the approach shown on the well-characterized TaAs crystal.

ACKNOWLEDGMENTS

We are grateful to S. Komorovsky for fruitful discussions and for his interest in a direct comparison of DFT with SCDFT, which inspired part of this work. J.K.D. acknowledges funding from the National Science and Engineering Research Council of the Government of Canada through a Postdoctoral fellowship (Application No. 545643).

-
- [1] H. Weyl, *Z. Phys.* **56**, 330 (1929).
 [2] L. Balents, *Physics* **4**, 36 (2011).
 [3] P. B. Pal, *Am. J. Phys.* **79**, 485 (2011).
 [4] S. Murakami, *New J. Phys.* **9**, 356 (2007).
 [5] S.-Y. Xu, Y. Xia, L. Wray, S. Jia, F. Meier, J. Dil, J. Osterwalder, B. Slomski, A. Bansil, H. Lin, R. J. Cava, and M. Z. Hasan, *Science* **332**, 560 (2011).
 [6] X. Wan, A. M. Turner, A. Vishwanath, and S. Y. Savrasov, *Phys. Rev. B* **83**, 205101 (2011).
 [7] B. Singh, A. Sharma, H. Lin, M. Z. Hasan, R. Prasad, and A. Bansil, *Phys. Rev. B* **86**, 115208 (2012).
 [8] A. K. Geim and K. S. Novoselov, in *Nanoscience and Technology: A Collection of Reviews From Nature Journals* (World Scientific, Singapore, 2010), pp. 11–19.
 [9] M. Z. Hasan and C. L. Kane, *Rev. Mod. Phys.* **82**, 3045 (2010).
 [10] X.-L. Qi and S.-C. Zhang, *Rev. Mod. Phys.* **83**, 1057 (2011).
 [11] A. A. Zyuzin and A. A. Burkov, *Phys. Rev. B* **86**, 115133 (2012).
 [12] C.-X. Liu, P. Ye, and X.-L. Qi, *Phys. Rev. B* **87**, 235306 (2013).
 [13] P. Hosur and X. Qi, *C. R. Phys.* **14**, 857 (2013).
 [14] S. A. Parameswaran, T. Grover, D. A. Abanin, D. A. Pesin, and A. Vishwanath, *Phys. Rev. X* **4**, 031035 (2014).
 [15] G. B. Halász and L. Balents, *Phys. Rev. B* **85**, 035103 (2012).
 [16] A. A. Zyuzin, S. Wu, and A. A. Burkov, *Phys. Rev. B* **85**, 165110 (2012).
 [17] T. Das, *Phys. Rev. B* **88**, 035444 (2013).
 [18] T. Ojanen, *Phys. Rev. B* **87**, 245112 (2013).
 [19] J. Liu and D. Vanderbilt, *Phys. Rev. B* **90**, 155316 (2014).
 [20] M. Hirayama, R. Okugawa, S. Ishibashi, S. Murakami, and T. Miyake, *Phys. Rev. Lett.* **114**, 206401 (2015).
 [21] G. Xu, H. Weng, Z. Wang, X. Dai, and Z. Fang, *Phys. Rev. Lett.* **107**, 186806 (2011).
 [22] A. A. Burkov and L. Balents, *Phys. Rev. Lett.* **107**, 127205 (2011).
 [23] S.-M. Huang, S.-Y. Xu, I. Belopolski, C.-C. Lee, G. Chang, B. Wang, N. Alidoust, G. Bian, M. Neupane, C. Zhang, S. Jia, A. Bansil, H. Lin, and M. Zahid Hasan, *Nat. Commun.* **6**, 7373 (2015).
 [24] H. Weng, C. Fang, Z. Fang, B. A. Bernevig, and X. Dai, *Phys. Rev. X* **5**, 011029 (2015).
 [25] S.-Y. Xu, I. Belopolski, N. Alidoust, M. Neupane, G. Bian, C. Zhang, R. Sankar, G. Chang, Z. Yuan, C.-C. Lee, S.-M. Huang, H. Zheng, J. Ma, D. S. Sanchez, B. Wang, A. Bansil, F. Chou, P. P. Shibayev, H. Lin, S. Jia, and M. Zahid Hasan, *Science* **349**, 613 (2015).
 [26] L. Yang, Z. Liu, Y. Sun, H. Peng, H. Yang, T. Zhang, B. Zhou, Y. Zhang, Y. Guo, M. Rahn, D. Prabhakaran, Z. Hussain, S.-K. Mo, C. Felser, B. Yan, and Y. L. Chen, *Nat. Phys.* **11**, 728 (2015).
 [27] B. Q. Lv, H. M. Weng, B. B. Fu, X. P. Wang, H. Miao, J. Ma, P. Richard, X. C. Huang, L. X. Zhao, G. F. Chen, Z. Fang, X. Dai, T. Qian, and H. Ding, *Phys. Rev. X* **5**, 031013 (2015).
 [28] B. Lv, N. Xu, H. Weng, J. Ma, P. Richard, X. Huang, L. Zhao, G. Chen, C. Matt, F. Bisti, V. N. Strocov, J. Mesot, Z. Fang, X. Dai, T. Qian, M. Shi, and H. Ding, *Nat. Phys.* **11**, 724 (2015).
 [29] J. Buckeridge, D. Jevdokimovs, C. R. A. Catlow, and A. A. Sokol, *Phys. Rev. B* **93**, 125205 (2016).
 [30] J. Buckeridge, D. Jevdokimovs, C. R. A. Catlow, and A. A. Sokol, *Phys. Rev. B* **94**, 180101(R) (2016).
 [31] M. Dadsetani and A. Ebrahimiyan, *J. Electr. Mat.* **45**, 5867 (2016).
 [32] B. Peng, H. Zhang, H. Shao, H. Lu, D. W. Zhang, and H. Zhu, *Nano Energy* **30**, 225 (2016).
 [33] Y. Sun, Y. Zhang, C. Felser, and B. Yan, *Phys. Rev. Lett.* **117**, 146403 (2016).
 [34] T. Ouyang, H. Xiao, C. Tang, M. Hu, and J. Zhong, *Phys. Chem. Chem. Phys.* **18**, 16709 (2016).
 [35] D. Grassano, O. Pulci, A. M. Conte, and F. Bechstedt, *Sci. Rep.* **8**, 3534 (2018).
 [36] C. A. C. Garcia, J. Coulter, and P. Narang, *Phys. Rev. Research* **2**, 013073 (2020).
 [37] R. Zu, M. Gu, L. Min, C. Hu, N. Ni, Z. Mao, J. M. Rondinelli, and V. Gopalan, *Phys. Rev. B* **103**, 165137 (2021).
 [38] M. Lu, Y. Guo, M. Zhang, H. Liu, and S. T. John, *Solid State Commun.* **240**, 37 (2016).
 [39] Y. Zhou, P. Lu, Y. Du, X. Zhu, G. Zhang, R. Zhang, D. Shao, X. Chen, X. Wang, M. Tian, J. Sun, X. Wan, Z. Yang, W. Yang, Y. Zhang, and D. Xing, *Phys. Rev. Lett.* **117**, 146402 (2016).
 [40] W. Kohn and L. J. Sham, *Phys. Rev.* **140**, A1133 (1965).
 [41] G. Vignale and M. Rasolt, *Phys. Rev. B* **37**, 10685 (1988).
 [42] K. Bencheikh, *J. Phys. A* **36**, 11929 (2003).
 [43] J. Kubler, K.-H. Hock, J. Sticht, and A. Williams, *J. Phys. F* **18**, 469 (1988).
 [44] M. K. Armbruster, F. Weigend, C. van Wüllen, and W. Klopper, *Phys. Chem. Chem. Phys.* **10**, 1748 (2008).

- [45] G. Scalmani and M. J. Frisch, *J. Chem. Theory Comput.* **8**, 2193 (2012).
- [46] J. K. Desmarais, S. Komorovsky, J.-P. Flament, and A. Erba, *J. Chem. Phys.* **154**, 204110 (2021).
- [47] J. K. Desmarais, J.-P. Flament, and A. Erba, *Phys. Rev. B* **101**, 235142 (2020).
- [48] J. K. Desmarais, J.-P. Flament, and A. Erba, *Phys. Rev. B* **102**, 235118 (2020).
- [49] S. Pittalis, G. Vignale, and F. G. Eich, *Phys. Rev. B* **96**, 035141 (2017).
- [50] A. Becke, *J. Chem. Phys.* **117**, 6935 (2002).
- [51] E. R. Johnson, R. M. Dickson, and A. D. Becke, *J. Chem. Phys.* **126**, 184104 (2007).
- [52] I. V. Tokatly, *Phys. Rev. Lett.* **101**, 106601 (2008).
- [53] E. Trushin and A. Görling, *Phys. Rev. B* **98**, 205137 (2018).
- [54] J. K. Desmarais, J.-P. Flament, and A. Erba, *J. Phys. Chem. Lett.* **10**, 3580 (2019).
- [55] A. D. Becke, *J. Chem. Phys.* **98**, 5648 (1993).
- [56] C. Adamo and V. Barone, *J. Chem. Phys.* **110**, 6158 (1999).
- [57] See Supplemental Material at <http://link.aps.org/supplemental/10.1103/PhysRevB.105.125108> for a description of our strategy of reduction of SCDFT xc functionals to SDFT ones and for a plot showing the effect of the fraction α of Fock exchange on the electronic band structure.
- [58] R. Dovesi, A. Erba, R. Orlando, C. M. Zicovich-Wilson, B. Civalleri, L. Maschio, M. Rérat, S. Casassa, J. Baima, S. Salustro, and B. Kirtman, *WIREs Comput. Mol. Sci.* **8**, e1360 (2018).
- [59] A. Erba, J. Baima, I. Bush, R. Orlando, and R. Dovesi, *J. Chem. Theory Comput.* **13**, 5019 (2017).
- [60] J. K. Desmarais, J.-P. Flament, and A. Erba, *J. Chem. Phys.* **151**, 074107 (2019).
- [61] D. Figgen, K. A. Peterson, M. Dolg, and H. Stoll, *J. Chem. Phys.* **130**, 164108 (2009).
- [62] H. Stoll, B. Metz, and M. Dolg, *J. Comput. Chem.* **23**, 767 (2002).
- [63] J. P. Perdew, M. Ernzerhof, and K. Burke, *J. Chem. Phys.* **105**, 9982 (1996).